

TRANSITION REGION DOWNFLOWS IN THE IMPULSIVE PHASE OF SOLAR FLARES

S. KAMIO, H. KUROKAWA, D. H. BROOKS, R. KITAI, AND S. UENO

Kwasan Observatory, Kyoto University, Yamashina-Ku, Kyoto 607-8471, Japan; kamio@kwasan.kyoto-u.ac.jp

Received 2004 November 11; accepted 2005 February 17

ABSTRACT

We present observations of four flares that occurred during coordinated observations between the Coronal Diagnostic Spectrometer (CDS) on board *SOHO* and the Domeless Solar Telescope (DST) at Hida Observatory. We studied the evolution of relative Doppler velocities in the flare kernels by using He I (3.5×10^4 K), O V (2.2×10^5 K), and Mg IX (1.0×10^6 K) spectra obtained with high time cadence (42 s) *SOHO* CDS observations and the H α monochromatic images obtained with the DST. We found that the transition region plasma of O V showed strong downward velocities up to 87 km s^{-1} simultaneously with the downflows in the lower temperature chromospheric emissions in He I and H α during the impulsive phase of all four flares. From these results we suggest that the downflows in the transition region and the chromosphere are a common feature in the impulsive phase of flares. For the Mg IX line we did not detect any significant change in velocity, which suggests that the 10^6 K plasma was close to the intermediate temperature between the upflowing plasma (10^7 K) and the downflowing plasma (10^4 – 10^5 K). These are important for understanding the dynamics of the solar atmosphere in response to the sudden energy deposition of a flare.

Subject headings: Sun: chromosphere — Sun: flares — Sun: transition region

1. INTRODUCTION

Chromospheric evaporation is believed to be responsible for sudden increases in H α and soft X-ray emissions during the impulsive phase of flares. According to the theory of chromospheric evaporation, high-energy particles generated in the flare flow along the magnetic field and penetrate into the dense plasma of the chromosphere. This leads to explosive heating of the plasma up to 10^7 K, and the “explosion” causes both upflow and downflow of the heated plasma, which should be observable at different heights in the solar atmosphere. Chromospheric evaporation was first proposed by Neupert (1968), and upflows and downflows during the impulsive phase of flares have been reported in previous papers.

Ichimoto & Kurokawa (1984) detected red asymmetry emission in H α spectra during a flare, which was identified as a downflow of 50 – 100 km s^{-1} in the chromosphere. They showed that the observed red asymmetry emission was not caused by the absorption of upflowing plasma, but the downward motion in the chromosphere. Shoji & Kurokawa (1995) studied the impulsive phase spectra of two typical flares, for which the H α , Ca II K, He I D₃, Na I D_{1,2}, and other metallic lines were simultaneously obtained. They found that H α , Ca II K and He I D₃ lines showed nearly the same downward velocities, the maximum of which ranged from 50 to 100 km s^{-1} , while Na I D_{1,2} and metallic line emissions showed smaller maximum downward velocities of 2 – 6 km s^{-1} .

Antonucci et al. (1982) found a blueshifted component in Ca XIX and Fe XXV spectra obtained with the bent crystal spectrometer on *SMM* during the impulsive phase and derived upflow velocities of 300 – 400 km s^{-1} . Strong upflows in the 10^7 K plasma during the impulsive phase of flares support the chromospheric evaporation model. The upflows at 10^7 K were also found by the Bragg Crystal Spectrometer (BCS; Culhane et al. 1991) on board the *Yohkoh* satellite. Wülser et al. (1994) studied a *GOES* X1.5 flare on 1991 November 15, which was observed by the *Yohkoh* satellite and the Mees Solar Observatory. They analyzed Ca XIX spectra obtained with *Yohkoh* BCS and detected

an upflow component of 250 km s^{-1} during the impulsive phase of the flare. The blueshift of the line core was found to be 50 km s^{-1} . Although *Yohkoh* BCS has no spatial resolution, the dominant sources of the Ca XIX emission were assumed to be the flare sites identified by the soft X-ray telescope (SXT) on *Yohkoh*. They also found redshifts of 19 – 42 km s^{-1} in the H α spectrum and claimed that the estimated momenta of upflow and downflow were balanced.

In the transition region around 10^5 K, both upflows and downflows have been reported in previous studies. Cheng & Tandberg-Hassen (1986) derived the velocity and density variation in the transition region using Si IV (8×10^4 K) and O IV (1.6×10^5 K) lines. They found downflows up to 20 km s^{-1} and density increases of a factor of 3 during the impulsive phase. However, they detected downflows in only four of seven flare kernels, so it was not clear whether these downflows were a general characteristic of flares or not. The wavelength scanning of the UVSP instrument on board *SMM* caused some ambiguity in the velocity determination during the rapidly changing flare because each wavelength position of the spectrum was observed at a different time.

The Coronal Diagnostic Spectrometer (CDS; Harrison et al. 1995) on board *SOHO* can acquire simultaneous spectra that, in principle, should allow a more reliable determination of velocity. Note that CDS cannot determine absolute velocities, so careful analysis of individual data sets is required to determine relative Doppler velocities and/or nonthermal line widths as accurately as possible (see, e.g., Brooks & Kurokawa 2004). Only a few results on the velocities in the transition region have been obtained from CDS observations so far.

Brosius (2003) studied the evolution of an M6.3 flare on 2001 June 15 observed with CDS. He obtained O III, O V, Mg X, and Fe XIX spectra in the temperature range of 10^5 – 10^7 K in sit-and-stare observations with a high time cadence of 9.8 s. He performed a multicomponent fit for O V (2.2×10^5 K) spectra during the impulsive phase and detected a 360 km s^{-1} upflow component and a 50 km s^{-1} downflow component simultaneously. Recently Brosius & Phillips (2004) studied an M2 flare on 2001

April 24 with a similar CDS program. They reported upflow velocities of 40 km s^{-1} in EUV lines of O III, O IV, O V, and He II during flare precursor events and downflow velocities of 40 km s^{-1} during the impulsive phase. They also observed upward velocities with *Yohkoh* BCS and suggested that these results reflect momentum balance between the hot upflowing and cool downflowing material. However, the CDS field of view (FOV) was limited to $4'' \times 240''$ in his observations and the spatial distribution was not studied.

Teriaca et al. (2003) analyzed a C1.1 flare on 2001 May 26 using *SOHO* CDS and a spectroheliograph at the Dunn Solar Telescope. They found oppositely directed flows in the same flare kernel at the beginning of the flare. Derived velocities were $30\text{--}40 \text{ km s}^{-1}$ downward for He I $\lambda 10830$, 100 km s^{-1} upward for O V, and $20\text{--}160 \text{ km s}^{-1}$ upward for Fe XIX ($8 \times 10^6 \text{ K}$). They calculated upward and downward momenta using typical density values and claimed that the estimated momenta are of the same order. However, the temporal evolution during the flare was not clear because their time cadence was about 5 minutes.

So far, no CDS observations with adequate temporal resolution and spatial coverage have been made during a flare, and the velocity evolution in the transition region temperature range during a flare has not been established yet. We present observations of several flares that occurred during coordinated observation with *SOHO* CDS and the Domeless Solar Telescope (DST) at Hida Observatory. Our observations are characterized by high time cadences, which are 42 s for *SOHO* CDS and 15 s for DST $H\alpha$ images, and simultaneous coverage of the chromosphere, transition region, and corona (Brooks et al. 2004). Although the CDS cadence is lower than Brosius (2003), we obtained a wider FOV (through raster observations), which provided the spatial distribution of the flare kernels. In § 2 we describe the observations, and in § 3 we present the data reduction procedures. The evolution of the flares and derived velocities are presented in § 4. In § 5 we discuss the evolutions of the transition region and chromosphere in the impulsive phase of the flares.

2. OBSERVATIONS

Coordinated observations between Hida DST and *SOHO* CDS were carried out from 2002 July 26 to August 9. In the DST, $H\alpha$ images were obtained with a Lyot filter of 0.25 \AA FWHM. The filter wavelength was shifted in the sequence of $-0.8, -0.5, +0.0, +0.5,$ and $+0.8 \text{ \AA}$ from $H\alpha$ line center, and the time cadence was 15 s for each wavelength. The spatial resolution was $0.5''$ at its best, although it varied with the seeing conditions.

The *SOHO* CDS program was designed to achieve a high time cadence of 42 s while retaining some spatial coverage. We used the normal incidence spectrometer (NIS) $4'' \times 240''$ slit and scanned an area of $16'' \times 240''$. Wide-field scans of $48'' \times 240''$ were taken every 50 scans, which were used for co-alignment with the DST $H\alpha$ images. Data were binned in the y -direction along the slit for the sake of high time resolution, and the spatial resolution after binning was $4'' \times 3.2''$. We selected the spectral lines He I $\lambda 584.33$ ($3.5 \times 10^4 \text{ K}$), O V $\lambda 629.73$ ($2.2 \times 10^5 \text{ K}$), and Mg IX $\lambda 368.06$ ($1.0 \times 10^6 \text{ K}$), covering the temperature ranges of the upper chromosphere, transition region, and low corona. These lines are among the strongest in the NIS spectra and are therefore suitable for high cadence studies.

During this observational campaign, four flares were simultaneously observed by the DST and CDS. In this paper we mainly discuss the results for the flare on 2002 August 7 and then com-

pare the findings with the results for the other flares. Although this is the smallest flare among the four flares, the seeing conditions at the DST were the best.

TRACE (Handy et al. 1998) 171 \AA images were available for the flares on July 28, 29, and 31. High-resolution data of *TRACE* are suitable for studying the structure of flare ribbons. The magnetic polarities of flare kernels are investigated using photospheric magnetic field measured by *SOHO* MDI (Scherrer et al. 1995). We used full disk data and their pixel size was $2''$.

The Nobeyama Radio Heliograph (NoRH; Nakajima et al. 1994) is a microwave interferometer, and daily 8 hr observations have been made since 1992 June. Spatial resolutions for synthesized data are $10''$ for 17 GHz and $5''$ for 34 GHz. We used spatially resolved data to obtain the microwave flux from particular active regions. The best temporal resolution of NoRH is 0.1 s, but 1 s accumulated data are used in the analysis.

3. DATA REDUCTION

The CDS data were debiased and calibrated and cosmic rays were removed using standard CDS software. The intensity maps were produced by integrating the spectra over each CDS spectral window, after the debias correction, flat fielding, and other standard corrections had been applied. Velocities were inferred by fitting the obtained spectra with broadened Gaussian post-recovery of *SOHO* line profiles (Thompson 1999) using the procedure ADAS-602, which is implemented in the Atomic Data and Analysis Structure package (ADAS; Summers 2003). CDS cannot measure the absolute wavelengths of the lines in our study so we derived only relative Doppler velocities on the assumption that the mean velocity of each individual image is 0. In addition, the inferred velocities show various systematic trends that should be removed, for example, a north-south bias due to spectral rotation and line tilt on the NIS detector. We corrected for these effects using a detailed data reduction procedure developed and described by Brooks & Kurokawa (2004). Internally consistent velocity maps were thus obtained, and the accuracy is expected to be higher than that derived using standard CDS procedures for correcting such north-south trends.

Because the Mg VII $\lambda 367.66$ ($6.7 \times 10^5 \text{ K}$) in the blue wing of Mg IX may enhance during the flare, we performed a two-component fit for Mg IX spectra. Although the fitted velocity of the weak Mg VII component is not reliable, the velocity fluctuation of Mg IX is reduced compared to the result from the one-component fit.

The DST images are stabilized by means of correlation tracking, which removes drift due to seeing conditions and solar rotation. We have tracked big sunspots in the DST images for this study because they can be identified in both the $H\alpha$ line-center and wing images. An accurate co-alignment for half an hour is required for this study, since we have focused on the evolution of preflare and impulsive phases. Although the shape of the sunspots changed in the course of the observations, they were stable during the time span of half an hour. The estimated error of the DST image alignment is about $1''$ for the data sets we have studied.

CDS and DST data are co-aligned by identifying common features in He I ($3.5 \times 10^4 \text{ K}$) wide FOV intensity maps and in the $H\alpha$ images. We do not use CDS pointing data for the co-alignment because they may contain the error of several arc-seconds. Although the spatial resolution of CDS is not as good as the DST data, dark filaments and plages can be identified in both the He I map and $H\alpha$. The accuracy of the co-alignment is expected to be better than 1 CDS pixel ($4'' \times 3.2''$).

4. RESULTS

4.1. Flare on 2002 August 7

A B7.7 (*GOES* soft X-ray classification) flare occurred in active region NOAA AR 10061 at 23:43 UT on 2002 August 7. Our observations started at 22:29 UT, so the preflare and impulsive rise of the flare were captured with CDS and the DST. The $H\alpha$ filter image with an overlying contour of the $He\ I$ intensity map is presented in Figure 1.

Five flare kernels were identified in the sequence of $H\alpha$ line-center images, which are labeled A–E in Figure 1, and their light curves are presented in Figure 2. The $H\alpha$ light curves are derived by integrating intensity over $2'' \times 2''$ boxes in Figure 1. The size of $2'' \times 2''$ is selected in order to track the evolution of small $H\alpha$ kernels. Weak brightenings occurred in kernels A and B at 23:37 UT (labeled 1), but kernels C, D, and E did not change at that time. Other brightenings were found in kernels C, D, and E at 23:41 UT (labeled 2) when the *GOES* soft X-rays showed a slight increase. The intensities of kernel A and B increased a little at the same time, but the amounts of the increase were smaller than the main peak of the flare. These two brightenings are thought to be precursor events of this flare. At 23:44 UT (labeled 3) the intensities of kernels A, B, and *GOES* soft X-ray increased rapidly, while kernels C, D, and E did not show any significant increase. The *GOES* soft X-ray light curve reached its peak at 23:45 UT and gradually decreased after that. After the impulsive peaks, the intensities of the $H\alpha$ kernels A and B increased until 23:48 UT and then decreased gradually.

Since $H\alpha$ kernels B and C were in the FOV of CDS, the evolutions of these two kernels are studied in detail. Light curves of *GOES* soft X-ray and NoRH 17 GHz are shown in the top panel of Figure 3. The time derivative of the *GOES* soft X-ray flux is used as a proxy for the hard X-ray flux (Neupert 1968). It showed a main peak at 23:43 UT and a less intense peak

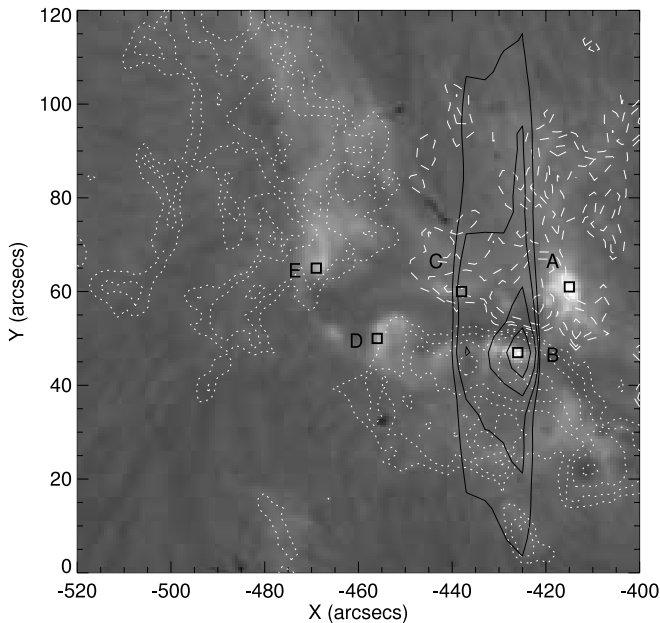


FIG. 1.— $H\alpha$ image showing the flare kernels at 2002 August 7 23:40:41 UT. Kernels A–E are marked by black squares. Overlaid solid contours indicate the $He\ I$ intensity map of *SOHO* CDS. Contour levels for $He\ I$ are 20, 40, 80, 160, 320, and 640 photon events $\text{pixel}^{-1} \text{s}^{-1}$. Dashed and dotted contours show positive and negative magnetic fluxes obtained from *SOHO* MDI data, respectively. Contour levels for MDI are -800 , -400 , -200 , -100 , 100 , 200 , 400 , and 800 G.

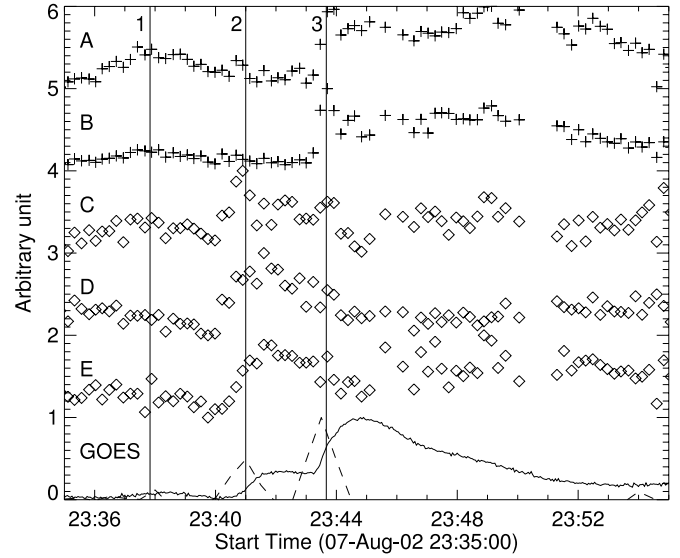


FIG. 2.—Light curves of the $H\alpha$ flare kernels and the *GOES* soft X-ray flux on 2002 August 7. Each light curve is normalized by its peak intensity. The locations of the $H\alpha$ kernels are indicated in Fig. 1. Three vertical lines indicate the times of the $H\alpha$ brightenings. The solid and dashed lines present the *GOES* soft X-ray flux and its time derivative.

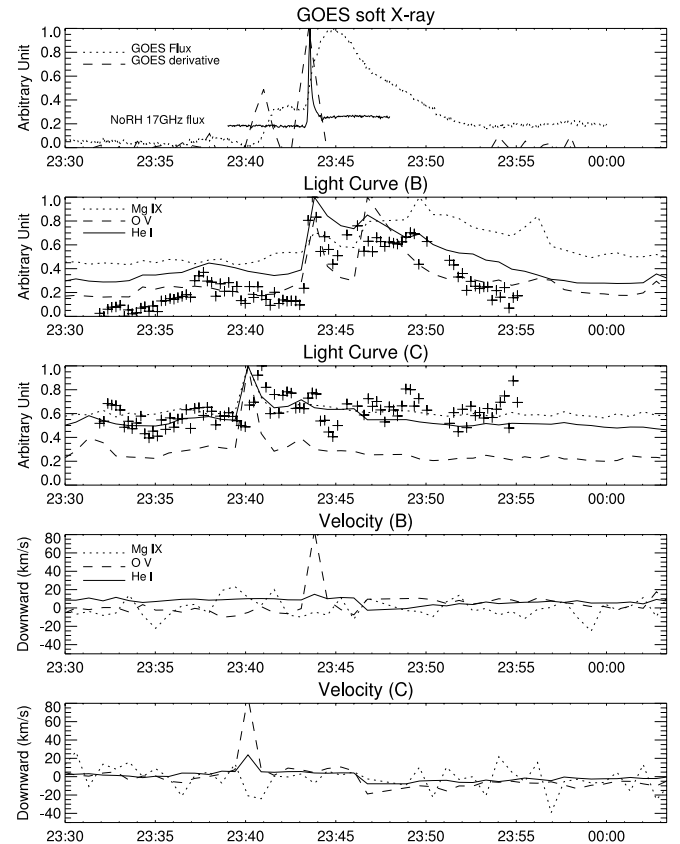


FIG. 3.—*Top*: *GOES* soft X-ray flux and its time derivative on 2002 August 7. The solid line shows the NoRH 17 GHz microwave flux in the active region. The middle two panels show light curves for kernels B and C. The dotted, dashed, and solid lines present the light curves of Mg IX, O V, and He I, respectively. Plus signs show the $H\alpha$ light curve for each kernel. The bottom two panels present line-of-sight velocities derived from Mg IX, O V, and He I spectra in kernels B and C. Downward motion (i.e., redshift in the spectra) is positive.

TABLE 1
PEAK VELOCITIES AND STANDARD DEVIATIONS

KERNEL	He I		O V		Mg IX	
	Velocity (km s ⁻¹)	σ (km s ⁻¹)	Velocity (km s ⁻¹)	σ (km s ⁻¹)	Velocity (km s ⁻¹)	σ (km s ⁻¹)
Jul 28.....	21	4.9	68	11	...	15
Jul 29.....	12	2.6	54	7.0	...	28
Jul 31 A.....	37	6.5	79	15	...	11
Jul 31 B.....	36	5.5	37	10	...	14
Aug 07 B.....	15	2.6	84	10	...	11
Aug 07 C.....	24	4.9	87	14	...	12

NOTES.—Peak velocities during the impulsive phase and standard deviations for each kernel pixel. Positive velocities indicate downflows. Only velocities exceeding 3σ levels are presented.

23:41 UT. In view of chromospheric evaporation, the soft X-ray flux represents the amount of evaporated plasma (10^7 K) and should reflect the amount of energy deposited into the chromosphere. The soft X-ray light curve suggests that the main energy release of the flare occurred around 23:44 UT.

One microwave source covering the whole active region was found in the NoRH data, so the microwave flux integrated over the active region is plotted in Figure 3. The NoRH 17 and 34 GHz fluxes reached their peak at 23:43:35 UT, which is really simultaneous with the peak in the soft X-ray flux derivative curve. This indicates that the soft X-ray derivative curve traces the evolution of the energy release quite well. The brightness temperature of 17 GHz flux exceeded 10^6 K, and the photon power-law index derived from NoRH 34 GHz/17 GHz flux was negative at the time of microwave burst. This implies that the microwave burst is due to gyrosynchrotron radiation by non-thermal electrons. The intensity peaks of H α kernels A and B were attained at 23:43:42 UT, the first exposure after the microwave burst. The timing coincidence of the microwave burst and the H α brightenings suggests that kernels A and B are related to the main energy release of the flare. Although EUV or X-ray observations of the flare loop were not available, kernels A and B were thought to be the footpoints of the same magnetic loop.

Kernel B was located in the narrow CDS FOV, and its light curves in He I, O V, and Mg IX are shown in Figure 3. These light curves are derived from the intensity of 1 CDS pixel corresponding to the H α flare kernel because H α data indicate that the size of the flare kernel is smaller than that of the CDS pixel ($4'' \times 3''.2$). The sudden intensity rises in H α coincided with the EUV brightening within the temporal resolution of the DST and CDS data, which were 15 and 42 s, respectively. The temporal relationship between the microwave burst and the brightening in H α and the EUV spectrum indicates that the evolution in the H α and the EUV reflects the chromospheric evaporation process.

Relative velocities at the flare kernels are plotted in Figure 3. As with the light curves, velocities of 1 CDS pixel are presented for each kernel. In the preflare phase, the intensity of He I slightly increased in kernel B from 23:34 to 23:38 UT, when the H α precursor was observed. No significant change was detected in the He I velocity at that time.

In kernel B, significant downflows of 15 and 84 km s⁻¹ were found in He I and O V, respectively, at 23:43:49 UT, while the velocity of Mg IX was about -5 km s⁻¹, below the 1σ level. The peak velocities in the flare kernel during the impulsive phase and velocity standard deviation are presented in Table 1. The standard deviations are calculated from the time series of the

velocity data at the kernel pixel. Only significant velocities greater than the 3σ level are shown in Table 1.

The strong downflows in He I and O V disappeared at 23:44:32 UT, which indicates that they lasted for less than 84 s of two exposures. These downflows coincided with the microwave burst and soft X-ray derivative peak and are thought to be the response to the energy deposition in the chromosphere and transition region.

The light curves and relative velocities for kernel C are also presented in Figure 3. The intensities of He I, O V, and Mg IX suddenly increased at 23:40:08 UT, and they went back to almost the preflare level in the next exposure at 23:40:52 UT. At the same time as the peak intensity, strong downflows of 24 and 87 km s⁻¹ were detected in He I and O V, respectively. Those downflows exceeded the 3σ levels and so are significant. The Mg IX line showed the velocity of -25 km s⁻¹, which is about 2σ and not significant enough to determine the upflow.

Figure 4 shows CDS spectra in kernel B at 23:43:49 UT, when the strong downflows in He I and O V were found. As mentioned in § 3, CDS cannot measure absolute wavelength, and the horizontal axis indicates the nonabsolute wavelength. It is shown that the He I and O V spectra are shifted redward from the preflare average and the line width decreased. This is interpreted as an emission enhancement of the redshifted component. In Mg IX, the blue wing around 368.0 was enhanced during the impulsive phase. This could be an upflow, but the derived velocity was not significant enough. The enhancement around 367.6 Å is due to Mg VII (6.7×10^5 K), which is removed in the velocity determination by means of a two-component fit.

The velocity in the chromosphere was estimated from a series of images in the H α line center and the ± 0.5 and ± 0.8 Å wings. We derived the excess intensities in the H α wing by subtracting the preflare intensities from those in the impulsive phase. In the H α wing, the emission from the chromosphere can be inferred by subtracting the preflare emission, which was assumed to be the constant photospheric emission. The intensity in the H α line core was excluded from this analysis because it was opaque and was only the emission from the upper chromosphere.

The inferred excess intensities in kernel B are marked by asterisks in Figure 5. Peak intensities in these four wavelengths were attained at different times from 23:43:44 to 23:48:55 UT because of the wavelength scanning of the H α filter. The intensity excess in $+0.8$ Å is larger than that in -0.8 Å, which agrees with previous observations of the red asymmetry of the H α profile in flares (Ichimoto & Kurokawa 1984). We estimated the downflow velocity in the chromosphere by fitting a second degree polynomial function. The estimated center of the excess

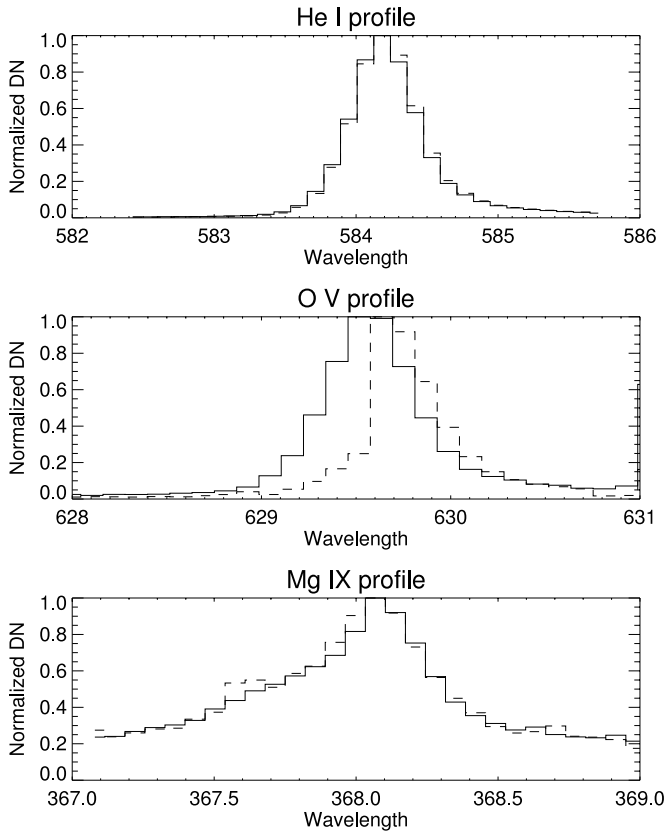


FIG. 4.—Dashed lines: *SOHO* CDS spectra at the pixel of kernel B at 23:43:49 UT; solid lines: preflare average from 23:36:28 to 23:40:08 UT. The horizontal axis indicates the (nonabsolute) wavelength scale in Å. Note that the dashed line spectra in He I and O V are redshifted and Mg IX shows an enhancement in the blue wing.

intensity profile shifted $+0.15 \text{ \AA}$ from $H\alpha$ center rest wavelength, which corresponds to a downward motion of 7 km s^{-1} .

However, this estimation may be inaccurate because it is derived from the intensity at only four wavelengths. Another problem is that the images in each wavelength were obtained at different times because they were taken by wavelength scanning of the filter. This causes ambiguity in the velocity deter-

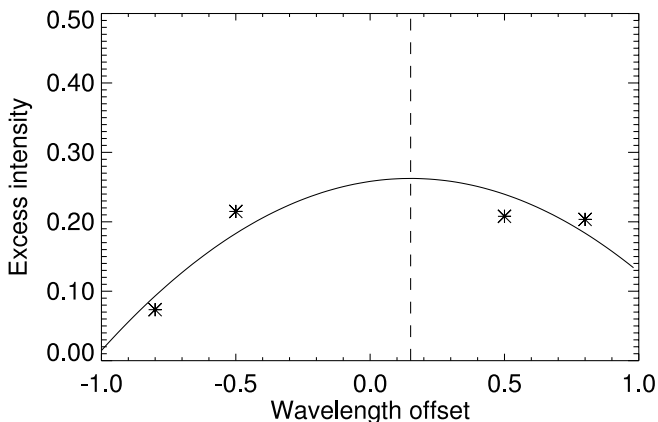


FIG. 5.— $H\alpha$ excess intensity profile for kernel B indicated by asterisks. The excess intensities are inferred by subtracting the preflare intensities in $H\alpha$ -0.8 , -0.5 , $+0.5$, and $+0.8 \text{ \AA}$ from those in the impulsive phase from 23:43:38 to 23:48:53 UT. The solid curve is a fitted second degree polynomial function. The estimated center wavelength is $+0.15 \text{ \AA}$, which corresponds to a redshift of 7 km s^{-1} .

mination during the flare that evolved in a very short time. Although the velocity estimation may therefore contain some errors, the obtained profile suggests that the red wing is more enhanced than the blue wing, and this indicates downflow in the chromosphere. If this estimation is correct, downflows were simultaneously detected in the chromosphere and transition region during this flare.

4.2. Flare on 2002 July 29

In NOAA AR 10039, a C4.2 class flare occurred on 2002 July 29. The DST seeing conditions during the impulsive phase were not so good because of bad weather. However, *TRACE* 171 Å data are available during the flare with a cadence of 40 s. Figure 6 shows an $H\alpha$ image right after the impulsive phase of the flare. The flare ribbons had developed well across the active region. Figure 7 presents *TRACE* 171 Å at 22:39:25 UT, when the first intensity peak was attained in kernel C. Overlaid contours indicate the CDS He I intensity map, which covered the flare ribbon in the east region.

Three $H\alpha$ kernels A–C were selected from visual inspection of the $H\alpha$ movie data. The kernel C on the edge of one of the flare ribbons was located in the CDS FOV. The southwest edge of the flare ribbon to which kernel B belonged was also found in the CDS FOV, but its intensity is much lower than that of kernel C. The photospheric magnetic field map from MDI shows that kernels B and C were located in a negative region and kernel A was found in a positive region. These $H\alpha$ kernels are also seen as bright spots in the *TRACE* 171 Å image in Figure 7. Kernel C is located near the footpoint of the transient bright loop that stretched in the southeast direction in the *TRACE* image at 22:39:25 UT. This suggests that kernel C was not directly connected to kernel A or B.

The *GOES* soft X-ray flux and CDS light curves for kernel C are presented in the top and the middle panels of Figure 8. The impulsive rise in He I, O V, and Mg IX at 22:38:50 UT coincides with the rapid increase of the soft X-ray flux, which suggests

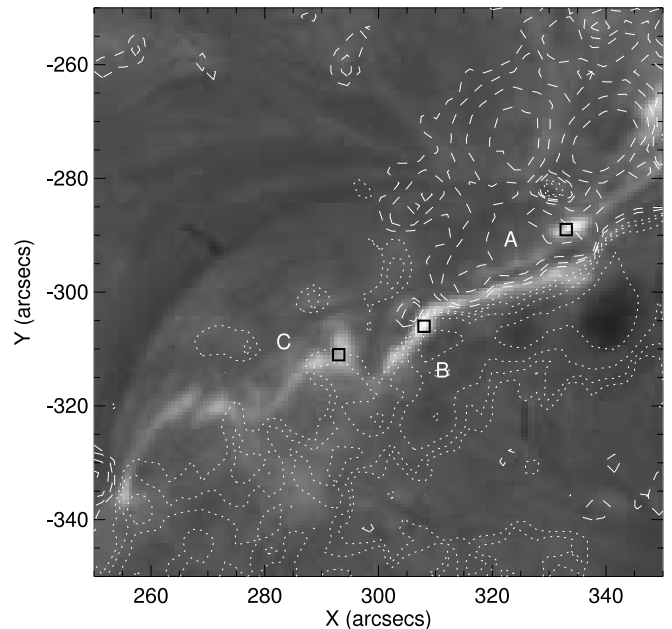


FIG. 6.— $H\alpha$ image showing the flare kernels at 2002 July 29 22:41:57 UT. Overlaid dashed and dotted contours show positive and negative magnetic fluxes obtained with *SOHO* MDI, respectively. Contour levels are the same as in Fig. 1.

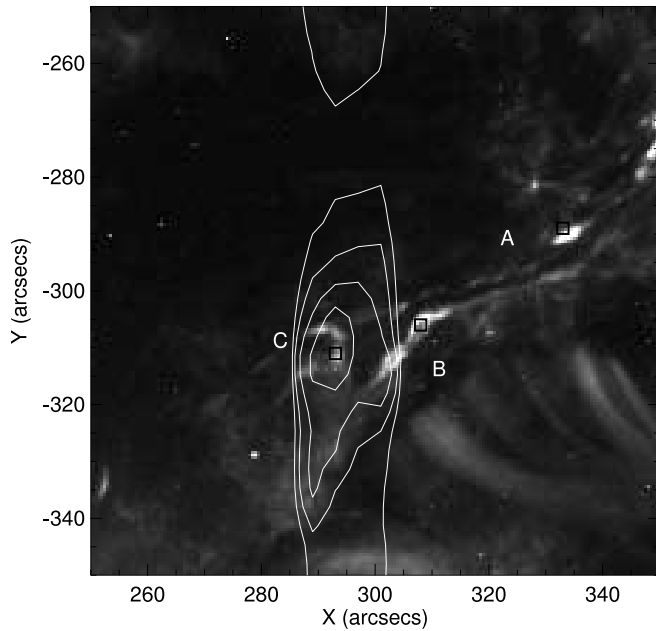


FIG. 7.—*TRACE* 171 Å intensity map at 2002 July 29 22:39:25 UT. The overlaid white contours indicate the *SOHO* CDS He I intensity map. Contour levels are the same as in Fig. 1.

that the dominant energy release occurred then. The bottom panel of Figure 8 shows velocities derived from the CDS spectrum. At the impulsive intensity peak at 22:38:50 UT, downward relative velocities of 12 and 24 km s⁻¹ are detected in He I and O V, respectively. These velocities exceed the 3 σ level and so are significant. In the next exposure of CDS at 22:39:35 UT, the velocity in O V increased to 54 km s⁻¹, but no significant downflow was found in He I. The velocities derived from Mg IX showed large fluctuations compared to He I and O V. No significant velocity was found in Mg IX around its peak at 22:38:50 UT. Its large standard deviation of 28 km s⁻¹ makes it difficult to determine significant flow, even though the velocity was derived by a two-component fit of Mg IX λ 368.06 and Mg VII λ 367.66.

After the first intensity peak, other intensity peaks were observed at 22:44 and 22:52 UT, but the derived velocities did not change in those peaks. They are thought to be episodic events and not related to the main energy release of the flare.

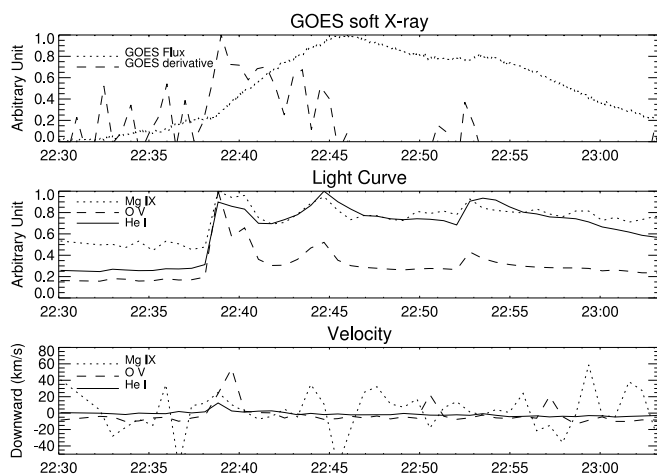


FIG. 8.—Light curves and derived velocities for kernel C in Fig. 6.

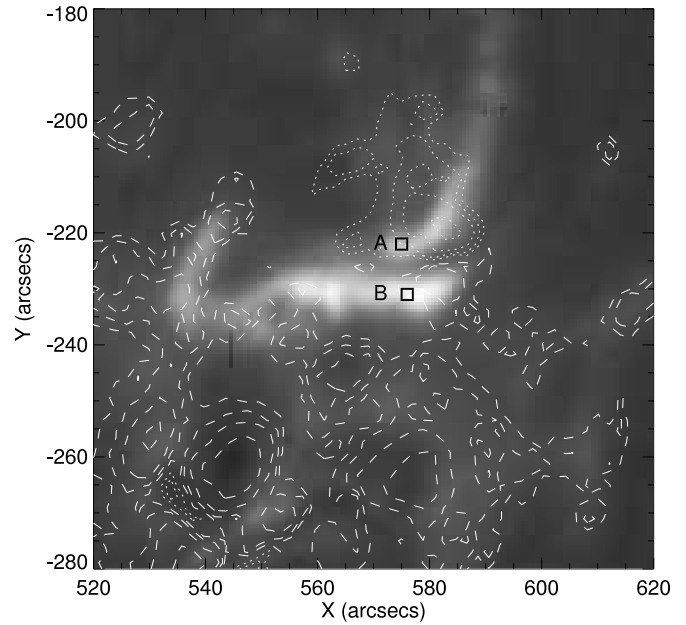


FIG. 9.— $H\alpha$ image at 2002 July 31 01:47:40 UT, the beginning of the flare. Dashed and dotted contours show positive and negative magnetic fluxes obtained with *SOHO* MDI, respectively. Contour levels are the same as in Fig. 1. Black squares indicate two intense kernels A and B.

4.3. Flare on 2002 July 31

An M1.2 class flare occurred in the north part of NOAA AR 10039 on 2002 July 31. Unfortunately, seeing conditions at the DST were not good during this flare and the observation was stopped in the decay phase because of bad weather. Figure 9 shows an $H\alpha$ image during the impulsive phase. Developing flare ribbons are identified in $H\alpha$. The most intense kernel in the negative polarity region was labeled A, and the most intense kernel in the positive polarity region was labeled B. Figure 10 presents a *TRACE* image and the He I contour in the impulsive phase, 13 s before the $H\alpha$ data in Figure 9. The connection

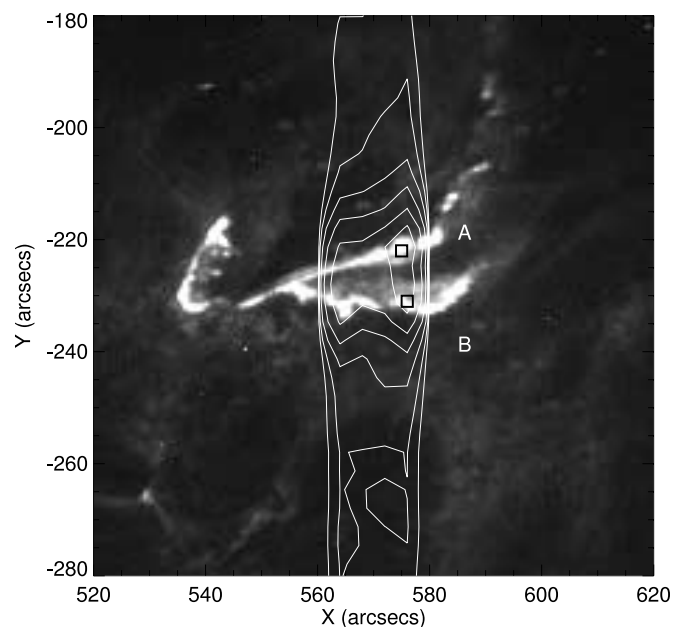


FIG. 10.—*TRACE* 171 Å image at 2002 July 31 01:47:27 UT. The overlaid contours indicate the *SOHO* CDS He I intensity during the impulsive phase.

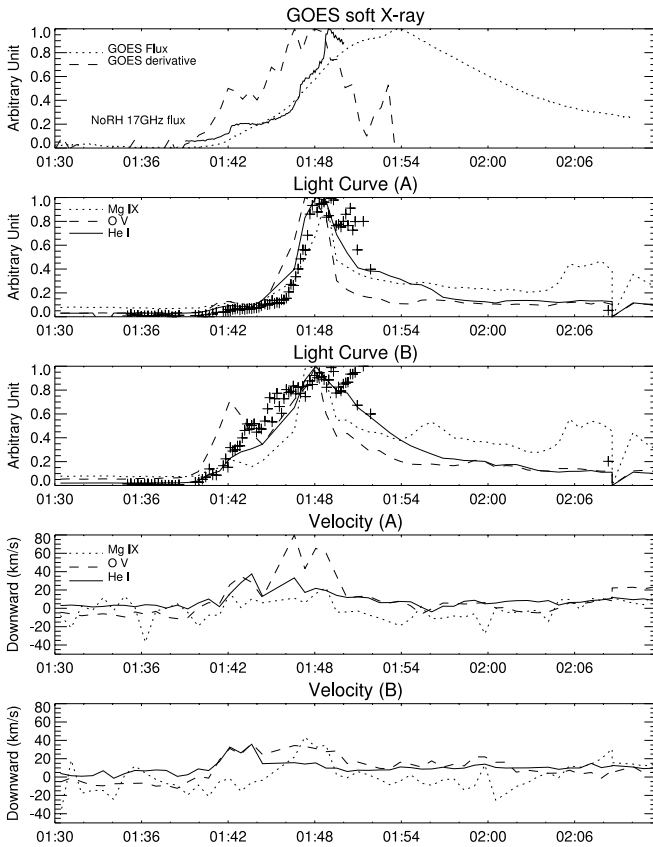


FIG. 11.—Light curves and derived velocities for kernels A and B in Fig. 9.

between these kernels is not apparent in *TRACE* 171 Å data, but the developing flare ribbons in H α and *TRACE* 171 Å look alike. The locations of H α intense kernels are indicated by black squares in Figure 10. They were cospatial with the flare ribbons in the 171 Å image.

Their light curves and the velocities at these kernels are presented in Figure 11. The first H α intensity increase was detected in kernel B around 01:40 UT, when the soft X-ray flux began to rise. The intensities in He I, O V, and Mg IX in kernel B also increased at the same time. In kernel B, downward velocities of 30 km s⁻¹ were detected in He I and O V at 01:42:07 UT, which coincides with the first O V intensity peak and the first impulsive burst in the soft X-ray derivative (hard X-ray proxy) curve. Note that the downward velocities in O V and He I showed the same evolution from 01:41 to 01:44 UT. This implies that the plasma motions in the O V and He I temperature ranges were strongly related. No significant velocity was found in Mg IX at that time.

In kernel A, downflows of 30 km s⁻¹ were detected in He I and O V at 01:42:53 UT. H α data were only available before 01:54 UT because of bad weather conditions, but the light curves of H α are similar to those of He I. The O V downflows increased to 80 km s⁻¹ by 01:46:35 UT, which coincided with the O V intensity peak. In He I, smaller but significant (20 km s⁻¹) velocities were detected at the same time. In the velocity curve of O V from 01:41 to 01:49 UT, three peaks are found at 01:42, 01:46, and 01:48 UT. These peaks coincided with the soft X-ray time derivative peaks in the top panel of Figure 11, and this implies that these downflow motions consisted of at least three short-lived events in kernel A. At 01:47:19 UT, significant velocity (43 km s⁻¹) was found in Mg IX in kernel B, but no significant flow was detected in He I.

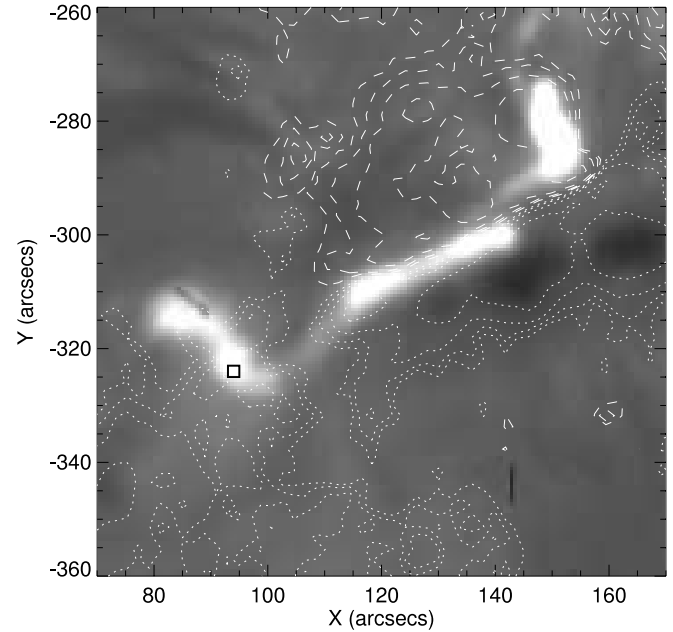


FIG. 12.—H α image at 2002 July 28 23:02:03 UT. Dashed and dotted contours show positive and negative magnetic fluxes obtained with *SOHO* MDI, respectively. Contour levels are the same as in Fig. 1.

4.4. Flare on 2002 July 28

An M1.1 class flare occurred in NOAA AR 10039 on 2002 July 28. Although the DST observations were interrupted by clouds, *TRACE* 171 Å data were available after the impulsive peak. Figures 12 and 13 show H α and *TRACE* 171 Å images after the impulsive phase. One of the flare kernels in a ribbon is identified in the contour of CDS He I. The flare kernel in the CDS FOV was located in a negative polarity region. CDS observed almost the same part of the active region as on 2002 July 29 (Fig. 6), although it had slightly changed in 1 day. Soft X-ray and 17 GHz microwave fluxes are presented in Figure 14. The soft

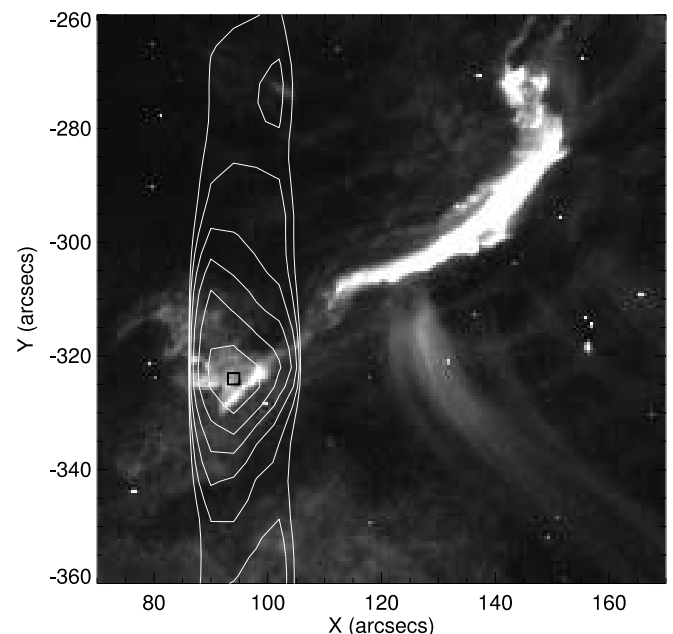


FIG. 13.—*TRACE* 171 Å image at 2002 July 28 23:08:02 UT and an overlaid contour of the *SOHO* CDS He I intensity map.

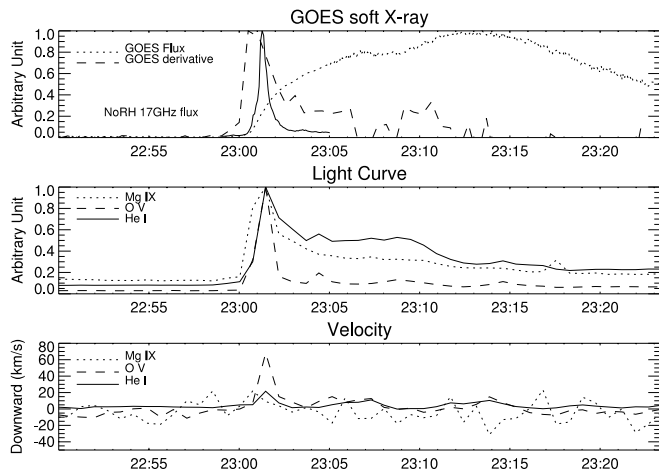


FIG. 14.—Light curves and derived velocities for the flare kernel on 2002 July 28.

X-ray derivative curve shows an impulsive peak between 23:00 and 23:02 UT, while the microwave flux reached its peak at 23:01:16 UT. Unfortunately, DST and *TRACE* data were not available in the impulsive peak time of 23:00–23:02 UT, so we analyzed only CDS data for this event. In Figure 14 the peak intensities of He I, O v, and Mg IX were attained at 23:01:28 UT. Downflows of 22 and 68 km s^{-1} were found in He I and O v, respectively. They exceeded the 3σ levels and diminished by the time of next exposure of CDS. While the intensities of Mg IX and O v in the kernel decreased gradually after their peak times, the soft X-ray flux increased until its peak at 23:12 UT.

5. DISCUSSION

Chromospheric evaporation is an important process for understanding the energy transportation in solar flares. Previously, downflows in the chromosphere (Ichimoto & Kurokawa 1984; Shoji & Kurokawa 1995) and upflows in the corona (Antonucci et al. 1982; Wülser et al. 1994) have been reported during the impulsive phase of flares. But the velocity evolution in the transition region (10^5 K) was obscure, since both upflows and downflows have been observed (Brosius & Phillips 2004; Teriaca et al. 2003). No observation with adequate spatial coverage and temporal resolution has been made with an EUV spectrometer. These motions are important for understanding the dynamics of the solar atmosphere in response to the sudden energy deposition in a flare.

We observed four flares ranging from *GOES* B7.7 to M1.2 class with *SOHO* CDS and Hida DST. In all four flares we observed, strong downflows up to 87 km s^{-1} were detected in O v (2.2×10^5 K), which coincided with a rapid increase of the soft X-ray flux. These results suggest that downflows at transition region temperatures are a common characteristic in the impulsive phase, regardless of the variety of the flare importance or the total flare energy. In the He I line (3.5×10^4 K) of the upper chromosphere, smaller but significant downflows up to 24 km s^{-1} were found. An $H\alpha$ profile estimation on 2002 August 7 gave a downflow of 7 km s^{-1} in the chromosphere (Fig. 5). In addition, the downflows also generally coincided with impulsive bursts in the microwave or soft X-ray derivative (a hard X-ray proxy) curves and vanished in less than 2 minutes. This suggests that these downflows in the upper chromosphere and transition region are related to the main energy release of the flare and must be distinguished from the so-called warm rain (Brosius 2003).

The warm rain, a falling plasma along the coronal loop, is observed in EUV lines or $H\alpha$ when evaporated plasma is cooled by conduction and radiation; thus, it should be observed after the impulsive phase.

We also found that the downflow velocities in O v do not depend on O v intensities. We can easily compare the intensities of different flares, since all four flares are observed and calibrated using the same programs. The O v intensity of the brightest pixel during the flare on 2002 July 28 was one order greater than that of 2002 August 7, but comparable downflow velocities of $60\text{--}80 \text{ km s}^{-1}$ were derived from O v spectra during these two flares.

The real downflow velocities in the impulsive phase may be larger than those derived from CDS data because the spectrum and inferred velocities give averages over the area of 1 pixel ($4'' \times 3''.2$). A chromospheric flare kernel consists of smaller flare points of less than $1''$ (Kurokawa 1989), and the comparison of $H\alpha$ and CDS data shows that the sizes of the $H\alpha$ flare kernels are smaller than the pixel size of the CDS observations. It is suggested that the structure of the flare kernel is not uniform over 1 CDS pixel in our observation, and higher spatial resolution is necessary to measure precise velocity.

Mg IX (10^6 K) did not show a significant change in velocity. At higher temperature, Wülser et al. (1994) found upflow components in Ca XIX (10^7 K), which is interpreted as evaporating plasma in the corona. Brosius (2003) claimed that the Fe XIX spectrum (8×10^6 K) obtained with *SOHO* CDS remained blue-shifted during the impulsive phase. Teriaca et al. (2003) inferred an upflow velocity of $-160 \pm 70 \text{ km s}^{-1}$ from multicomponent fitting of Fe XIX spectra but detected no significant velocity in Fe XVI (2×10^6 K). While we do not have the data in a high temperature range (10^7 K), we tentatively suggest that Mg IX did not show any significant changes in velocity because the Mg IX plasma of 10^6 K could be close to the intermediate temperature between upflows and downflows.

But it must be noted that we need more precise measurements of the 10^6 K plasma velocity by using other suitable spectral lines. A two-component fit was carried out for Mg IX $\lambda 368.06$ spectra in order to compensate the possible enhancement of Mg VII $\lambda 367.66$ in the blue wing of Mg IX, but the derived velocity may be affected by noise because Mg IX spectra were less intense than He I and O v spectra. Although the velocity for Mg IX was below the detection limit in our study, more accurate measurement is required in future observations.

The numerical simulation (Fisher et al. 1985a, 1985b, 1985c) demonstrated that explosive evaporation occurs at high-energy flux of nonthermal electrons and upflow in the high-temperature corona and downflow in the chromosphere were expected in the case of explosive evaporation. They also estimated 40 km s^{-1} downflow in the transition region (10^5 K), which agrees with the downflows in O v in our observation, although our derived velocities are slightly larger. Brosius & Phillips (2004) detected upflows and downflows simultaneously during the impulsive phase and claimed that they were consistent with the simulation of explosive evaporation. Since we have no data for the temperature higher than 10^6 K, a higher temperature spectral line is necessary in future observations to confirm their result.

6. CONCLUSIONS

We studied the evolution of the kernels in four flares that occurred during coordinated observations between the *SOHO* CDS and the DST at Hida Observatory. The spatial distribution and temporal evolution of flare kernels were investigated by

using $H\alpha$ monochromatic images obtained with the DST. We derived relative Doppler velocities in the flare kernels from He I (3.5×10^4 K), O V (2.2×10^5 K), and Mg IX (1.0×10^6 K) spectra obtained with high time cadence (42 s) CDS observations.

We found that the transition region plasma of O V showed strong downward velocities up to 87 km s^{-1} , which coincided with the downflows in He I and $H\alpha$ in the chromosphere during the impulsive phase of flares. The downflows in the chromosphere have been detected from the spectroscopy of chromospheric line emissions during the flare (Ichimoto & Kurokawa 1984; Shoji & Kurokawa 1995), and they are thought to be the downward motion caused by the chromospheric evaporation. Our results indicate that the downflows in the transition region are also a common feature in the impulsive phase of flares.

For the coronal temperature range, upflows at 10^7 K have been reported (Antonucci et al. 1982; Wülser et al. 1994), but we did not detect any significant change in velocity for the Mg IX line. It suggests that the 10^6 K plasma is the intermediate between the upflowing plasma (10^7 K) and the downflowing plasma (10^4 – 10^5 K). These results are important for understanding the dynamics in the chromospheric evaporation process.

Our observational program was aimed at high time cadence (42 s), but high-speed downflows were detected in only one exposure. More precisely, the downflows in these flares were transient phenomena and lasted less than the 84 s of two exposures. We would have missed the transient flow if we had selected a slower observational program. We found downflows lasting about 5 minutes for the flare on 2002 July 31, but peaks in light curves and velocities suggest that they were made up of short-lived downflow events rather than a single event. Even higher time resolution is needed to study the detailed evolution of the chromospheric evaporation process. *Solar-B*, scheduled to be launched in 2006, will allow us to measure more accurate

Doppler velocity ($\pm 3 \text{ km s}^{-1}$) with the EUV Imaging Spectrometer (EIS). We will be able to study the dynamics in a flare kernel more precisely with the high spatial resolution of EIS (pixel size of $1''$).

The chromospheric evaporation can occur not only in the flares but also in the smaller events such as X-ray jets. Miyagoshi & Yokoyama (2003) carried out two-dimensional MHD simulation of coronal jets in the emerging flux region. They demonstrated that the chromospheric evaporation was essential for producing high-density jets. These small-scale events are important in terms of the mass supply and the energy transport in the corona.

Spectroscopic observations of the chromospheric lines are necessary to investigate the detailed evolution in the chromosphere. Previously, several papers have been published on that subject; however, simultaneous spectroscopy of the chromosphere, the transition region, and the corona will bring us better understanding of the chromospheric evaporation and energy transport process in the solar atmosphere.

We would like to thank A. Fludra for his help in planning the CDS observations. We would also like to thank the anonymous referee for improving our paper. This work is supported by the Grant-in-Aid for the 21st Century COE “Center for Diversity and Universality in Physics” from the Ministry of Education, Culture, Sports, Science, and Technology (MEXT) of Japan. CDS was built and is operated by a consortium led by Rutherford Appleton Laboratory and including Mullard Space Science Laboratory, the NASA Goddard Space Flight Center, Oslo University, and the Max Planck Institute for Extraterrestrial Physics, Garching. *SOHO* is a mission of international cooperation between ESA and NASA.

REFERENCES

- Antonucci, E., et al. 1982, *Sol. Phys.*, 78, 107
 Brooks, D. H., & Kurokawa, H. 2004, *ApJ*, 611, 1125
 Brooks, D. H., et al. 2004, *ApJ*, 602, 1051
 Brosius, J. W. 2003, *ApJ*, 586, 1417
 Brosius, J. W., & Phillips, K. J. H. 2004, *ApJ*, 613, 580
 Cheng, C.-C., & Tandberg-Hassen, E. 1986, *ApJ*, 309, 421
 Culhane, J. L., et al. 1991, *Sol. Phys.*, 136, 89
 Fisher, G. H., Canfield, R. C., & McClymont, A. N. 1985a, *ApJ*, 289, 414
 ———. 1985b, *ApJ*, 289, 425
 ———. 1985c, *ApJ*, 289, 434
 Handy, B. N., et al. 1998, *Sol. Phys.*, 183, 29
 Harrison, R. A., et al. 1995, *Sol. Phys.*, 162, 233
 Ichimoto, K., & Kurokawa, H. 1984, *Sol. Phys.*, 93, 105
 Kurokawa, H. 1989, *Space Sci. Rev.*, 51, 49
 Miyagoshi, T., & Yokoyama, T. 2003, *ApJ*, 593, L133
 Nakajima, H., et al. 1994, *Proc. IEEE*, 82, 705
 Neupert, W. M. 1968, *ApJ*, 153, L59
 Scherrer, P. H., et al. 1995, *Sol. Phys.*, 162, 129
 Shoji, M., & Kurokawa, H. 1995, *PASJ*, 47, 239
 Summers, H. P. 2003, *The ADAS Manual*, Version 2.6, <http://adas.phys.strath.ac.uk>
 Teriaca, L., Falchi, A., Cauzzi, G., Falciani, R., Smaldone, L. A., & Andretta, V. 2003, *ApJ*, 588, 596
 Thompson, W. T. 1999, *CDS Software Note 53*, Version 1 (Greenbelt: GSFC)
 Wülser, J.-P., Canfield, R. C., Acton, L. W., Culhane, J. L., Phillips, A., Kosugi, T., & Tsuneta, S. 1994, *ApJ*, 424, 459